

Constant current corona triode with grid voltage control. Application to polymer foil charging

José A. Giacometti and J. Sinézio Carvalho Campos


Citation: [Review of Scientific Instruments](#) **61**, 1143 (1990); doi: 10.1063/1.1141438

View online: <http://dx.doi.org/10.1063/1.1141438>

View Table of Contents: <http://scitation.aip.org/content/aip/journal/rsi/61/3?ver=pdfcov>

Published by the [AIP Publishing](#)

For all your variable temperature, solid state characterization needs....
... delivering state-of-the-art in technology and proven system solutions for over 30 years!



The advertisement features the MMR Technologies logo on the left. Below it are four images of scientific instruments: a microscope-like device labeled 'Solutions for Optical Setups!', a Seebeck measurement system, a variable temperature microprobe system, and a Hall measurement system. At the bottom, contact information is provided: Email: sales@mmr-tech.com, Web: www.mmr-tech.com, Phone: (650) 962-9622, and Fax: (833) 522-1011.

MMR TECHNOLOGIES

Seebeck Measurement Systems

Variable Temperature Microprobe Systems

Hall Measurement Systems

Email: sales@mmr-tech.com Web: www.mmr-tech.com Phone: (650) 962-9622 Fax: (833) 522-1011

Constant current corona triode with grid voltage control. Application to polymer foil charging

José A. Giacometti

Instituto de Física e Química de São Carlos, Universidade de São Paulo, Caixa Postal 369, CEP 13560, São Carlos, SP, Brasil

J. Sinézio Carvalho Campos

Departamento de Física, Universidade Estadual Paulista Julio Mesquita Filho, CEP 13500, Rio Claro, SP, Brasil

(Received 19 September 1989; accepted for publication 21 November 1989)

A new version of a corona triode setup, allowing charging dielectric foils with a constant current, was developed. The charging current is kept constant by controlling the grid voltage. We show that the sample surface potential can be inferred from the grid voltage and present results of the uniformity of charge deposition during the charging procedure. Sample charging currents could be varied from 1 to 300 nA/cm² and the foils could be charged up to ± 6 kV. The method was applied to measure the potential buildup on Teflon FEP and PVDF samples and these results are discussed. They showed that the method can be successfully applied to study the polarization buildup of β -PVDF foils under corona charging.

INTRODUCTION

The dynamics of the transport of extrinsic charge in polymeric dielectrics containing no intrinsic carriers, is dominated by transfer of free charge and charge trapping. In spite of numerous investigations, considerable uncertainty remains about the value of carrier mobility, density of traps, the process of trap-filling, and the presence of charge in surface states. A variety of methods has been used to investigate the discharge process of dielectrics previously charged by electron injection¹ or a high-voltage corona.² We believe that additional information can be gained from methods that allow one to follow the entire charging and discharging cycle of a sample, from its initial charge-free condition to the final steady, charged or charge-free state. This type of measurement is possible with electron-beam charging,³ and with the use of a corona system in which the charging current can be measured and, preferentially, controlled.

Using a three-electrode corona system, hereafter called corona triode, one is able to measure the charging current and the surface voltage of the sample during the charging process and the subsequent surface voltage decay in open circuit.⁴ The surface voltage is measured by using the method of the vibrating capacitor. A special version of this triode has been developed^{5,6} in which the charging current is controlled and kept constant at a desired value. Such a system resembles an electron gun, which also operates at constant charging current, but it has the advantage of providing for positive as well as for negative currents.

The method proved to be an excellent tool for the study of conduction phenomena in highly insulating polymers.⁵⁻¹² For instance, the electric transport properties of Teflon FEP at room temperature were successfully investigated.⁸⁻¹² It was shown that at the start of the charging, the negative charge is heavily trapped on the sample surface, while at a later stage it is trapped in bulk, until traps become almost saturated.

Recently, it was shown that the corona triode with constant current could be improved if the current control is performed using a grid voltage control.¹³⁻¹⁵ In a previous paper,¹⁵ one of us developed a model for such a corona triode describing mainly the dynamics of the charging process yielding a surface charge distribution as uniform as possible. In this article, we describe a new version of a corona triode setup having an improved performance. The range of the charging currents is between 1 and 300 nA/cm² and the samples can be charged up to ± 6 kV. Section I describes the experimental setup and Secs. II and III show the experimental technique employed to keep the charging current constant and to determine the sample surface potential from the measurement of the grid voltage instead of using the vibrating capacitor technique.⁴ Section IV shows that an improved charge uniformity over the sample surface can be achieved with this setup. To finalize we show results of the potential buildup for the polymers Teflon FEP and PVDF proving that the technique is a very efficient tool for the study of the polarization of β -PVDF samples under corona charging. A qualitative discussion of the charge transport and polarization is also made for PVDF samples.

I. EXPERIMENTAL SETUP

Figure 1 shows the schematic diagram of the experimental setup for the corona triode. The corona charging system consists of the corona pin electrode P and a metal cylinder connected to the variable high-voltage sources (Alpha III, Brandenburg) V_c and V_{ci} (Fluke model 410B), respectively. These voltage supplies and the metal grid G are biased by a controlled voltage supply V_g (model 152, Monroe Electronics Inc.). Both supplies V_g and V_c are operated in the constant current mode. The stainless-steel grid had a 500- μ m spaced mesh with wires of 50- μ m diam. The distance between the corona point and the grid could be adjusted but in our measurements was usually kept at 6 cm, unless other-

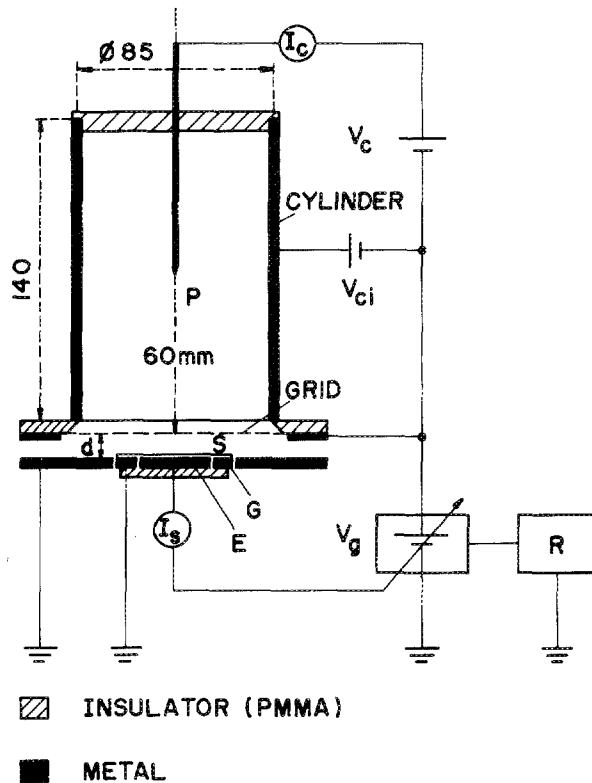


FIG. 1. Schematic diagram of the corona triode system. V_c and V_g are controlled power supplies; V_{ci} a voltage supply; I_c and I_s are ammeters; R a pen recorder. S the sample, G is the guard ring, and E the measuring electrode. All dimensions are in millimeters and d is the distance between the grid and the sample.

wise stated. The sample S stretched between two metallic rings is mounted on a sample holder and the distance d between grid and sample holder could be adjusted. A guard ring G prevents the surface currents from reaching the measuring electrode. The area of the measuring electrode is $A = 2.5 \text{ cm}^2$, the inner diameter of the guard ring is 2.1 cm and the outer diameter is 4.2 cm. One surface of the sample, of thickness L , is uncoated; the other is covered by an evaporated aluminum coating. The guard ring is connected to ground and the measuring electrode to the feedback current input of the controlled supply V_g . A battery operated electrometer I_s (model 602 Keithley Instrum.) and an ammeter I_c are used for monitoring the sample charging current $I(t)$ and the corona current I_c . The output voltage of the supply V_g is measured using the recorder R . The polarity of the supplies can be reversed in order to allow the samples to be charged with currents of both polarities.

II. CURRENT CONTROL AND SAMPLE POTENTIAL MEASUREMENT

The analysis presented here aims to show how the sample charging current $I(t)$ can be kept constant at a value I_0 and how the sample voltage can be inferred from the measured grid voltage $V_g(t)$. Figure 2 shows the region of interest of the triode comprised between the grid and the sample holder. For the sake of simplicity, we assume that the electric

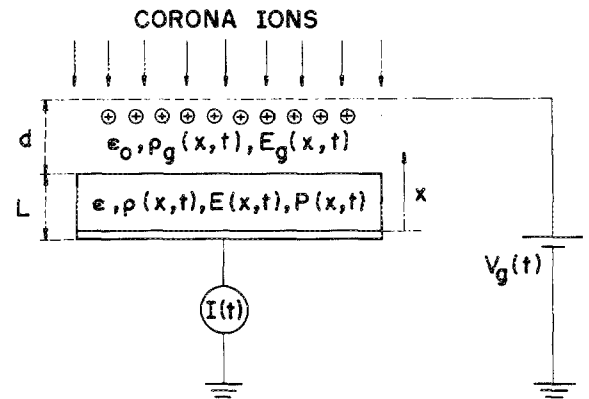


FIG. 2. Schematic diagram of the sample and the air gap below the grid with indication of quantities. Here ϵ and ϵ_0 are the dielectric constants; $E(x,t)$ and $E_g(x,t)$ the electric fields; $\rho(x,t)$ and $\rho_g(x,t)$ the charge densities; $P(x,t)$ the electric polarization; x the position; L and d the sample thickness and the air gap width, respectively; $V_g(t)$ the grid voltage and $I(t)$ the charging current.

quantities are independent of the lateral position in the air gap (one-dimensional geometry). It is known that the air gap conduction current is due to the transport of an ionic excess charge with a density $\rho_g(x,t)$.¹⁵⁻¹⁷ The total charging current density $J(t) = I(t)/A$, A being the sample area, is given by

$$J(t) = [v + \mu E_g(x,t)] \rho_g(x,t) + \frac{\epsilon_0 \partial E_g(x,t)}{\partial t}, \quad (1)$$

where the term $v\rho_g(x,t)$ is the current density due to the gas displacement produced by the corona discharge (corona wind). $E_g(x,t)$, μ , and ϵ are, respectively, the gap electric field, the ion mobility, and the air dielectric constant.

Integrating Eq. (1) over the air gap thickness, we have

$$J(t) = \frac{1}{d} \int_L^{L+d} [v + \mu E_g(x,t)] \rho_g(x,t) dx + \frac{\epsilon_0}{d} \frac{d}{dt} [V_g(t) - V(t)], \quad (2)$$

where $V_g(t) - V(t) = V_s$ is the air gap potential drop due to the ionic space charge. So, whenever V_s is experimentally kept constant, a stationary state for the ionic charge density and the electric field is reached in the air gap. Then, Eq. (2) shows that the charging current density $J(t) = J_0 = I_0/A$ is independent of time and equal to the mean value of the conduction current, which is the first term on the right side of Eq. (2). In the inverse way, keeping the current J_0 constant implies a constant voltage drop V_s in the gap.

Experimentally, the charging current is kept constant by using a constant current supply V_g . As Fig. 1 shows the charging current $I(t)$ is fed into the feedback input of the current supply and its value can be monitored with the floating electrometer. Then, measuring the voltage $V_g(t)$ of the current supply necessary to keep $I(t) = I_0$ we can determine the sample potential, as discussed in the later paragraph, by the relation

$$V(t) = V_g(t) - V_s, \quad (3)$$

if V_s is known. Since the amount of gap space charge is de-

pendent on the corona current I_c it is necessary to keep its value independent of the charging time. We recall that this is done by using the supply V_c operating in the constant current mode, Fig. 1.

Therefore, the setup proposed in this article both allows one to control the ion flux to the sample surface and to determine the sample potential during the charging by measuring $V_g(t)$. We point out that the sample potential during the charging cannot be measured by using the technique of the vibrating capacitor⁴ since the potential difference between the grid and the sample is constant. Of course, after charging, the vibrating capacitor can be used but such measurements will not be discussed here.

III. THE CALIBRATION CURVES FOR SAMPLE POTENTIAL DETERMINATION

In order to determine the sample surface potential from Eq. (3) it is necessary to know the air gap potential drop V_s as a function of system parameters and measurement conditions. The measurements of the air gap current density J_0 vs V_s , hereafter called calibration curves, were performed without a dielectric sample in the sample holder. Therefore, the measured V_g equals the value of V_s .

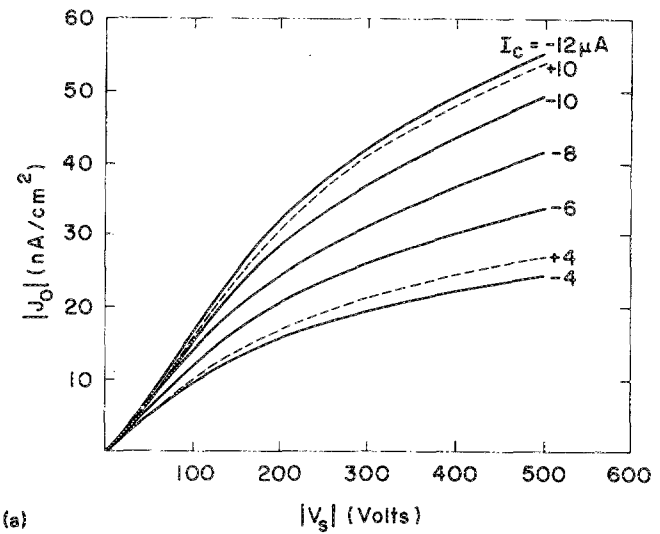
Figure 3 shows the calibration curves for several values of the corona current I_c for both corona polarities. The results show that J_0 increases as a function of I_c due to the fact that the dielectric transparency of the grid increases as a function of I_c (the grid transparency is proportional of the electric field above the grid¹⁶). Then, to assure the correctness of the $V(t)$ determination during a charging process we must keep I_c at a fixed value, otherwise an error will be introduced in Eq. (3) due to the variation of V_s as a function of I_c . In the experimental setup, the electrical field in the charging region of the corona (above the grid) is kept independent of the variable bias V_g by using a biased supply V_c for the corona discharge, Fig. 1. The supply V_c is operated in the constant current mode, thus assuring a constant value for the corona current I_c . Figure 3 also shows that the results are dependent on the corona polarity and for simplicity we show only two curves for the positive corona (dashed lines).

All the calibration curves have the common feature of not crossing the origin. Figure 3(b) shows a detail of curves near the origin. This effect happens due to the fact of the corona wind being proportional to the square root of the corona current.¹⁸

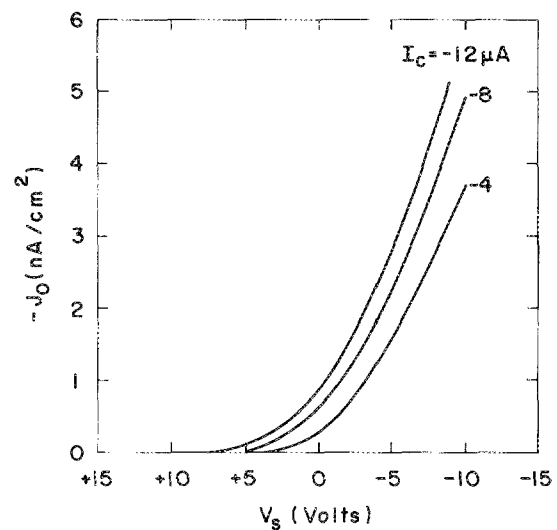
Calibration curves were also determined as functions of the other system parameters. Figure 4 shows the dependence of the curves with the distance d between the grid and the sample for the negative polarity. Short distances give higher currents than larger ones since the air gap ionic conduction current is determined by Child's law,¹⁹ being proportional to $d^{-3/2}$.

Figures 3 and 4 were obtained with current densities up to 80 nA/cm², but using small values for the air gap width and high values for the corona current; the setup can be operated up to 300 nA/cm².

Figure 5 shows the effect of temperature on the calibration curves for the negative corona. Increasing the temperature of the air gap medium decreases the ion mobility and



(a)



(b)

FIG. 3. (a) Calibration curves: charging current density J_0 vs the space charge potential drop V_s in the air gap for several corona currents I_c of both polarities. Corona point to grid distance: 6 cm; grid to sample surface distance: $d = 3$ mm. The dashed lines represent the curves for the positive polarity. (b) Current density behavior near the origin showing that for $V_s = 0$ the value of J_0 is different from zero (corona wind effect). Measurement conditions are the same as for Fig. 3(a).

thus the gap current. Similar results are obtained for the positive polarity.

IV. SURFACE POTENTIAL UNIFORMITY DURING CHARGING

It is interesting to recall that the most important feature of the constant current corona triode setup with grid voltage control is the improved surface potential uniformity.¹⁵ The good uniformity is attained by the metal cylinder and mainly by the existence of the ionic space charge in the air gap and the auto-compensation effect produced by the sample charges. A detailed discussion of this process and the dynamics of charge buildup can be found in Ref. 15.

In this article, we measured the potential uniformity of charged samples by scanning a Teflon FEP sample surface

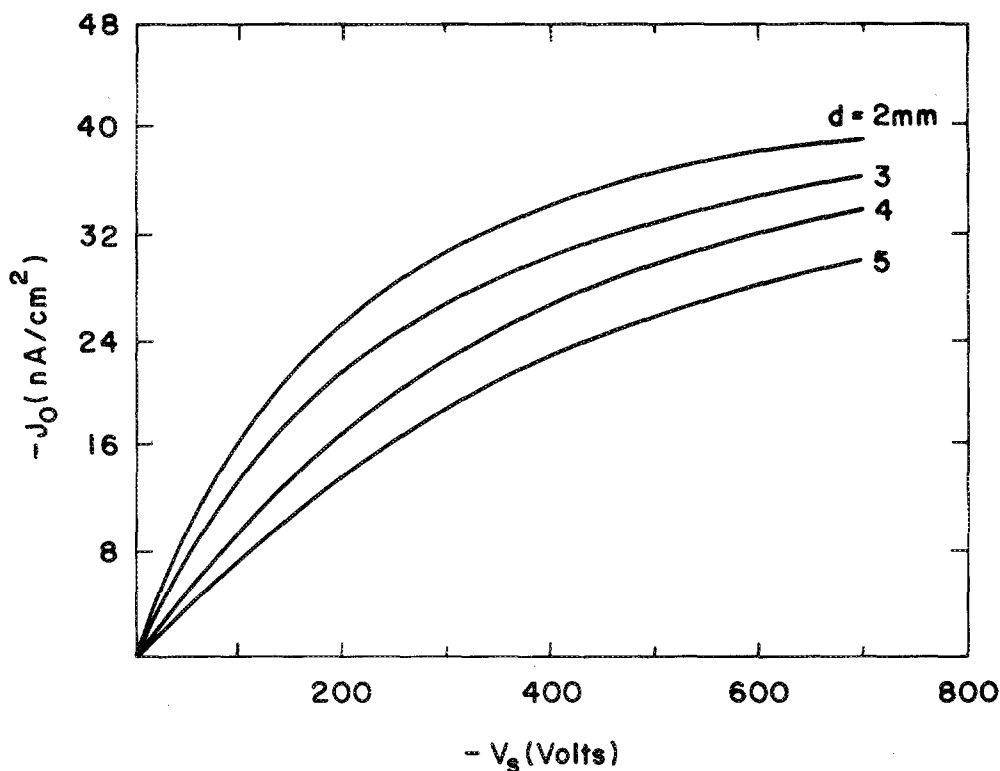


FIG. 4. Calibration curves: charging current density J_0 vs the space charge potential drop V_s in the air gap as a function of the grid to sample distance d . Corona current: $I_c = -10 \mu\text{A}$; corona point to grid distance: 6 cm.

with an electrostatic vibrating probe (Monroe, model 144S-4). The negative sample potential of Teflon FEP samples does not decay within the measurement time involved here.⁹ As shown by the curves of Fig. 6 the sample potential increases almost uniformly as a function of charging time (the measurements were done by interrupting the charging). For high values of the sample voltage, the uniformity decreases near the edges of the sample probably due to the

charge deflection induced by the field lines which reach the ground plate around the sample (see the schematic drawing of the setup in Fig. 1). We point out that better uniformity is achieved when using small currents (low V_s) and a short air gap.

This kind of measurement also allows one to compare the value of the sample potential measured with this setup with the one measured by the electrostatic probe. The values

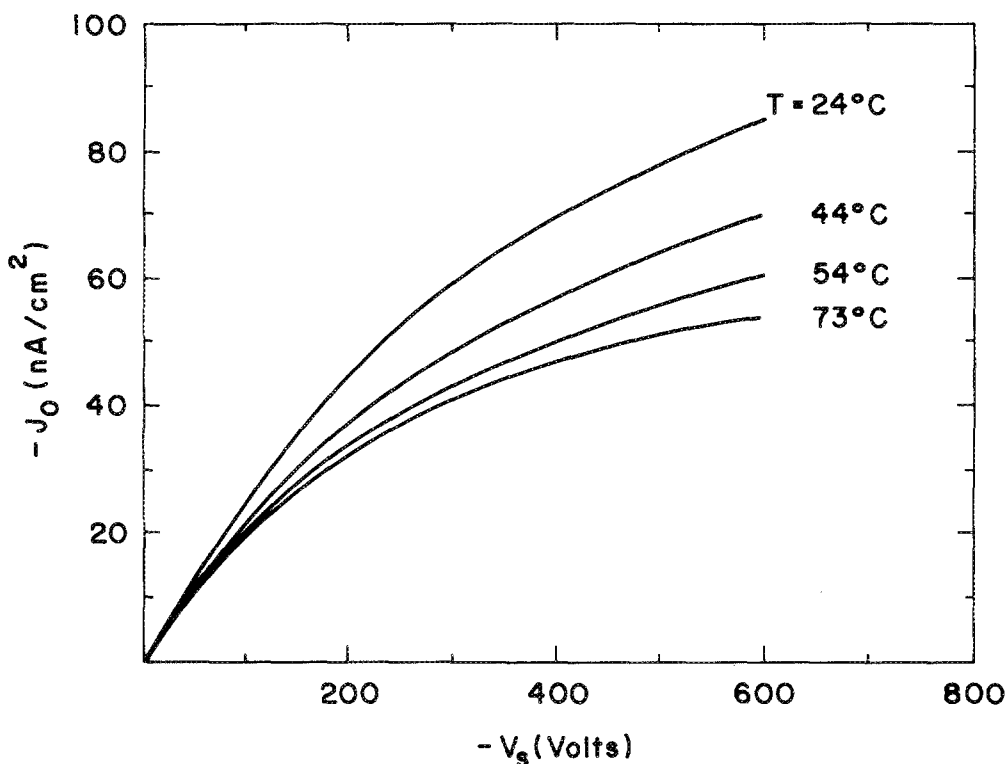


FIG. 5. Calibration curves: charging current density J_0 vs the space charge potential drop V_s in the air gap as a function of the air temperature. Corona current $I_c = -10 \mu\text{A}$; corona point to grid distance: 6 cm; grid to sample distance: $d = 3 \text{ mm}$.

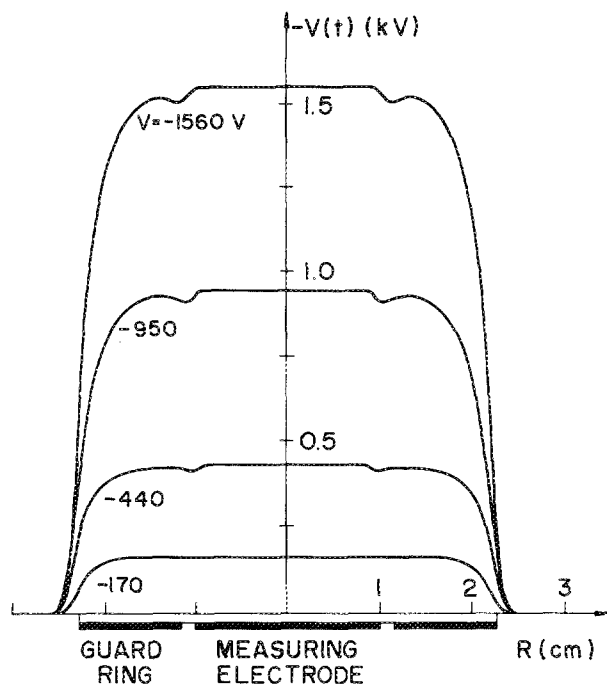


FIG. 6. Surface charge distribution on a Teflon FEP sample as a function of the radial position during the charging process. The sample was $25\ \mu\text{m}$ thick and it was negatively charged with $J_0 = 16\ \text{nA}/\text{cm}^2$. Corona current $I_c = -6\ \mu\text{A}$; corona point to grid distance: 6 cm; grid to sample distance: $d = 3\ \text{mm}$. The values indicated in the curves corresponds to the measured ones with the corona setup.

marked in Fig. 6, obtained from Eq. (3), show an agreement of the order of 2% with the values measured with the Monroe probe.

V. POTENTIAL BUILDUP ON TEFLON FEP

The total current density $J(t)$ in the sample can be written as

$$J_0 = J_c(x,t) + \frac{\partial D(x,t)}{\partial t}, \quad (4)$$

where $J_c(x,t)$ is the conduction current density and $D(x,t)$ the electric displacement. Since Teflon FEP is a nonpolar material, $D(x,t) = \epsilon E(x,t)$, ϵ being the dielectric permittivity. Because there is no current leakage through the bulk (when charged negatively at moderate surface charge density⁹), we can impose that $J_c(x,t) = 0$. Thus, after an integration of Eq. (4) over x we get

$$I_0 = C \frac{dV(t)}{dt}, \quad (5)$$

where $C = \epsilon A/L$ is the sample capacitance.

Figures 7 and 8 correspond to the experimental results for FEP samples with several thicknesses and charged negatively with different charging currents. The sample potential increases linearly as a function of time in agreement with Eq. (5), independently of charging current and sample thickness, which allows one to determine the sample capacitance C from Eq. (5). Table I shows a comparison between the sample capacitance values C calculated from Eq. (5) by using the rate of increase of the potential, and the value C_b

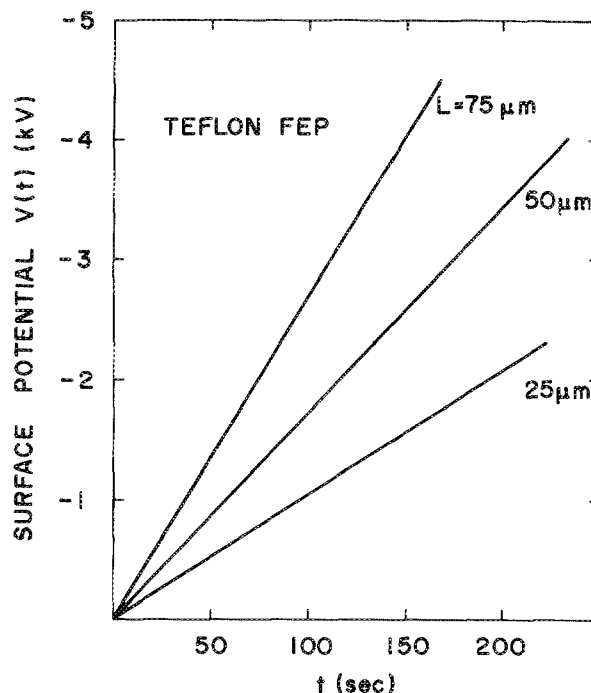


FIG. 7. Potential buildup for Teflon FEP samples charged negatively with a current density $J_0 = -0.67\ \text{nA}/\text{cm}^2$. The sample thicknesses are indicated in the figure. Corona current: $I_c = -4\ \mu\text{A}$; corona point to grid distance: 8 cm; grid to sample surface distance: $d = 5\ \text{mm}$.

measured using a capacitance bridge. We found that the values of C and C_b agree within 3%.

Measurements performed with this corona triode setup showed that we can charge foils up to $\pm 6\ \text{kV}$, the upper limit being determined by the Paschen breakdown in the system and by the insulation of the floating supplies and the insulators of the assembling parts of the system.

VI. POTENTIAL BUILDUP FOR PVDF

Figures 9 and 10 show the potential buildup for α - and β -PVDF samples. Figure 9 shows that for the α -PVDF the sample potential $V(t)$ increases to a maximum value, subsequently decreases, and again increases until it reaches a stationary state whose value is equal to the previous maximum value. If the neutralization of the surface charge is performed and then the sample is charged for the second time, $V(t)$ increases monotonously to a saturation value. For a β -PVDF sample, in the first charging process, the potential increases at the beginning up to a certain value, maintains

TABLE I. Comparison between the sample capacitance values C_b measured with a bridge capacitance and the values C determined by the rate $dV(t)/dt$ of the potential increase, Eq. (4). The data were taken from Fig. (7). Teflon FEP samples charged negatively with $J_0 = 0.67\ \text{nA}/\text{cm}^2$.

Sample thickness (μm)	C_b (pF)	C (pF)	Deviation (%)
75	132	136	3
50	204	200	2
25	344	352	2

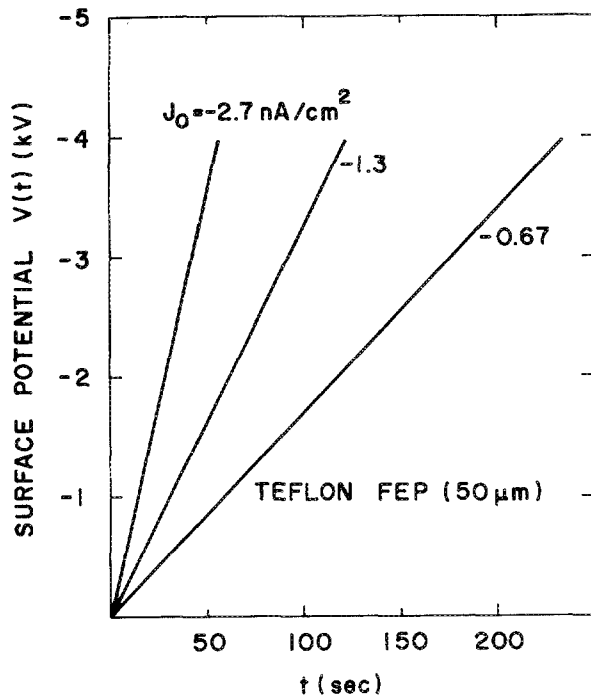


FIG. 8. Potential buildup for a Teflon FEP sample with 50 μm thickness charged with the various current densities which are indicated in the figure. Corona current $I_c = -4 \mu\text{A}$; corona point to grid distance: 8 cm; grid to sample surface distance: $d = 5 \text{ mm}$.

this value for some time, and then increases to a saturation value. During the second charging the potential increases monotonously to the steady state. The results of Figs. 9 and 10 show the salient difference between the potential buildup of a weakly polar α -PVDF sample and a strong polar β -PVDF sample.

A qualitative explanation for the results is given as follows. For α foils the potential increases up to a certain value and subsequently decreases due to a dipolar orientation,

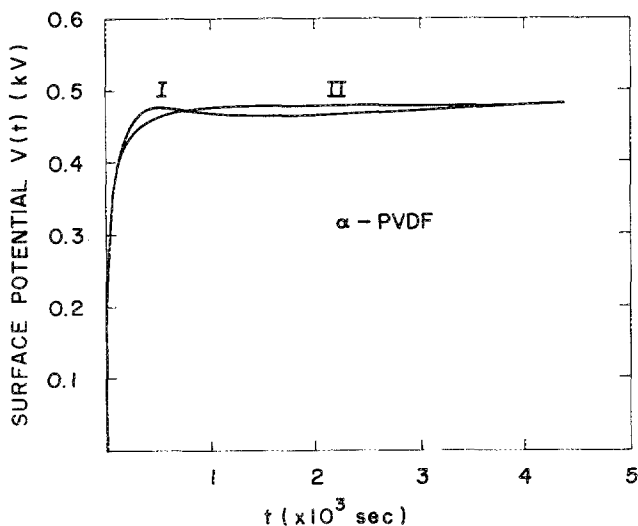


FIG. 9. Potential buildup for α -PVDF sample 15 μm thick charged with $J_0 = -44 \text{ nA/cm}^2$. Curve I corresponds to the first charging process and curve II to a second charging with the same polarity after a surface charge neutralization.

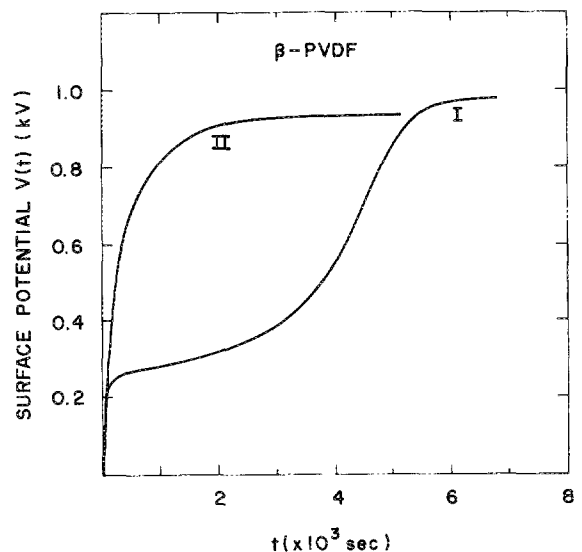


FIG. 10. Potential buildup for a β -PVDF sample 10 μm thick charged with $J_0 = +16 \text{ nA/cm}^2$. Curve I corresponds to the first charging process and curve II to a second charging with the same polarity after a surface charge neutralization.

probably of the type t^{-n} . When the electric polarization is completed, $V(t)$ starts to increase again until the steady state is reached due to the charge leakage through the sample. For β samples, $V(t)$ increases up to a critical value where polarization orientation starts. Afterwards, dipolar orientation neutralizes the charge deposited on the sample and thus prevents the potential to increase. When the ferroelectric polarization reaches the saturation value, the potential increases to the steady-state value. After the charging process, the samples have a permanent polarization and a second charging process is determined by the charge leakage through the sample only. The measured steady-state potential V_0 depends on the square root of the charging current density J_0 indicating that the conduction process is due to space-charge injection and not due to an ohmic conductivity as was observed for PVDF at very low electric fields.⁷ We point out that for the case of α samples, the first potential buildup could be reproduced if the sample is stored for several days before the second charging run.

We found that the potential buildup of the PVDF samples is almost independent of the charging polarity and that the leakage current through α -PVDF is higher than through β samples. The estimate of the mobilities for PVDF will be given in the next section.

VII. DISCUSSION

A comparison between the setup described in this article and the old version used to obtain the results described in Refs. 5–12 is made mainly considering two aspects: the uniformity of the charging deposition and the wide charging current. Although in the old version, the uniformity of the surface charge distribution was sufficient to give adequate measurements of the sample potential during charging, the new setup has a much superior performance. The charge uniformity here is much better than the previous one and it

can be achieved using a metal grid with a single mesh rather than with the double grid used before.⁴ The improved charge uniformity is attained due to the existence of the ionic space charge in the gap between the grid and the sample. During measurement, the gap potential drop V_s is small and the conduction current through the gap is limited by the space charge. A perfect uniformity can be achieved when the space-charge limited current condition (SCLC) is obtained over the whole width of the gap. A complete discussion of the charging dynamics is given in Ref. 15. The charging current with the previous setup is limited to 10 nA/cm² since the current is kept constant controlling the corona voltage (increasing the corona voltage increases the corona current, the ions being "forced" to reach the sample) and using a constant value for the grid voltage.⁷ This fact does not permit one to increase the charging current easily since very high values for corona voltage are necessary which are not practical from an experimental point of view. Also, since the grid voltage is fixed at a certain value, the sample cannot be charged to a value higher than V_g . In the version described here, there is no such restriction and the sample could be charged until Paschen breakdown occurred in the air or in the insulating parts of the setup or the sample ruptured. We have with this system charged samples up to ± 6 kV with charging currents up to 300 nA/cm².

High values for the charging current allow one to charge samples with a large capacitance like PVDF. Section VI showed the results for this polymer obtained with the new setup. We believe that it is a reliable and convenient method which could make a large contribution to the comprehension of the corona poling phenomena, mainly for the piezoelectric and pyroelectric polymers used for industrial applications.²⁰ Several attempts have been made to try to understand the corona poling of PVDF (Refs. 21 and 22) but none of the techniques employed was powerful enough to control the corona charging process or to give all the quantities necessary to clarify the poling process.

Results from Sec. V make it clear that for Teflon FEP, the charge deposited on the sample remains on its surface since the sample potential increases linearly with time. For values of the sample surface, charge densities higher than used here charge injection into the sample bulk could occur and such a phenomenon is well discussed in Refs. 8–11.

From the results in Sec. VI, it is clear that the dipolar orientation occurs mainly on β -PVDF sample. Before discussing the polarization, it is interesting to clarify the conduction process through the sample. The experimental results show that the stationary sample potential V_0 is a function of J_0^1 indicating space charge conduction (SCLC) (Ref. 19) and not an ohmic conductivity observed only at very low fields.⁷ This square-root dependence was observed for α - and β -PVDF samples but with the difference that for the α sample, the conduction current is much higher than for the β sample. Using the expression $J_0 = (9/8)\mu\epsilon V_0^2/L^3$ one can determine the carrier mobilities for both samples.¹⁹ Using the results of Figs. 9 and 10 we have $\mu_\alpha = 3.2 \times 10^{-10}$ cm²/V s and $\mu_\beta = 9.3 \times 10^{-12}$ cm²/V s. It is also interesting to note that the experimental results showed that the mobil-

ity is independent of the charging polarity for both kinds of PVDF.

If one attributes the region of the charging curve I of Fig. 10 where the potential is nearly constant as a function of time, to a uniform polarization through the sample, the value of the latter can be determined as follows. The total charge density deposited on the sample is $J_0 t$, t being the charging time. One part of it is neutralized by the reorientation of the dipoles and the other part drifts to the back electrode. Therefore, the polarization reversal is given by: $P = (J_0 - J_c)t_c/2$, t_c being the time where $V(t)$ remains constant and J_c the conduction current. Using values taken from curve II of Fig. 10, $t_c = 2700$ s, $\mu_\beta = 9.3 \times 10^{-12}$ cm²/V s, $V(t) = 350$ V, $J_0 = 16$ nA/cm², $J_c = (9/8)\mu\epsilon V^2/L^3 = 1.8$ nA, one has $P = 19$ μ C/cm². This estimated value seems to be higher than the permanent polarization value mentioned in the literature.^{23,24} A possible explanation for such a difference is that during the corona poling, not only the ferroelectric polarization occurs but also a time-dependent nonpermanent polarization, in agreement with another work.²⁵ Measurements of the piezoelectric activity in β -PVDF samples gave a reasonable value for the d_{31} coefficient. A value of 20 pC/N was measured on the sample whose poling curve is shown in Fig. 10.

It was demonstrated that the corona triode setup with constant current charging is a powerful tool to study the corona poling of polymer foils. The new setup shows that a highly uniform surface charge distribution can be achieved during the poling and that a large range of charging currents could be used. The large current allows one to pole thin β -PVDF samples and obtain a reasonable piezoelectric activity. The results for PVDF give a very clear picture of the orientation of the polarization in the sample. A complete discussion of the potential buildup of α - and β -PVDF samples will be given in another work.

ACKNOWLEDGMENTS

The authors express their thanks to Conselho Nacional de Desenvolvimento Científico e Tecnológico (CNPq) and to TELEBRAS for financial support, and to Bernhard Gross for helpful discussions.

¹B. Gross, *Top. Appl. Phys.* **33**, 217 (1980).

²G. M. Sessler, *Top. Appl. Phys.* **33**, 13 (1980).

³B. Gross, G. M. Sessler, and J. E. West, *J. Appl. Phys.* **45**, 284 (1974).

⁴R. A. Moreno and B. Gross, *J. Appl. Phys.* **47**, 3397 (1976).

⁵B. Gross, J. A. Giacometti, G. F. Leal Ferreira, and R. A. Moreno, in *Proceedings of Second Japan-Brazil Symposium on Science and Technology*, 13–16 October, 1980, Rio de Janeiro, pp. 166.

⁶J. A. Giacometti, Ph.D. Thesis, Universidade de São Paulo, 1982 (in Portuguese).

⁷B. Gross, J. A. Giacometti, G. F. Leal Ferreira, and O. N. Oliveira, Jr., *J. Appl. Phys.* **56**, 1487 (1984).

⁸B. Gross, J. A. Giacometti, and G. F. Leal Ferreira, in *Proceedings of Conference on Electrical Insulation and Dielectric Phenomena-IEEE*, 25–28 October, 1981, Whitehaven, PA, IEEE Publ. 81 CH1668-3 (IEEE, Piscataway, NJ, 1981), p. 39.

⁹J. A. Giacometti, G. F. Leal Ferreira, and B. Gross, *Phys. Status Solidi A* **88**, 297 (1985).

¹⁰B. Gross, J. A. Giacometti, and G. F. Leal Ferreira, *Appl. Phys. A* **37**, 89 (1985).

- ¹¹G. F. Leal Ferreira and O. N. Oliveira, Jr., *Phys. Status Solidi A* **105**, 531 (1988).
- ¹²B. Gross, J. A. Giacometti, and G. F. Leal Ferreira, *IEEE Trans. Nucl. Sci.* **28**, 4513 (1981).
- ¹³R. Haug, French Patent Specification 8414209.
- ¹⁴J. A. Giacometti and J. S. Carvalho Campos, in *Proceedings of the 6th International Symposium on Electrets*, 1–3 Sept. 1988, Oxford England, edited by D. K. Das-Gupta and A. W. Pattullo (IEEE, Piscataway, NJ, 1988), pp. 404–408.
- ¹⁵J. A. Giacometti, *J. Phys. D* **20**, 675 (1987).
- ¹⁶R. Haug, J. Lebas, and Y. Teisseyre, *J. Phys. D* **17**, 357 (1984).
- ¹⁷O. N. Oliveira, Jr. and G. F. Leal Ferreira, *Rev. Sci. Instrum.* **56**, 1957 (1985).
- ¹⁸M. Robinson, *Trans. Am. Inst. Electr. Eng.* **80**, 143 (1961).
- ¹⁹M. A. Lampert and P. Mark, in *Current Injection in Solids* (Academic, New York, 1970).
- ²⁰T. T. Wang and J. M. Hebert, Eds., *The Applications of Ferroelectric Polymers* (Blackie, London, 1988).
- ²¹P. D. Southgate, *Appl. Phys. Letters*. **28**, 250 (1976).
- ²²R. Gerhard-Multhaupt, in *Proceedings of the 4th International Conference on Dielectric Materials, Measurements and Applications* (IEE, London, 1984), pp. 53–56.
- ²³T. T. Wang and J. E. West, *J. Appl. Phys.* **53**, 6552 (1982).
- ²⁴M. A. Marcus, *Ferroelectrics* **32**, 149 (1981).
- ²⁵B. Gross, R. Gerhard-Multhaupt, A. Berraisoul, and G. M. Sessler, *J. Appl. Phys.* **62**, 1429 (1987).